SCIENTIFIC REPORTS

OPEN

SUBJECT AREAS:
SURFACES, INTERFACES AND THIN FILMS
TWO-DIMENSIONAL MATERIALS

Received
13 May 2014

Accepted
2 September 2014

Published
6 October 2014

Correspondence and requests for materials should be addressed to F.X. (fjxu@pku.edu.cn) or B.S. (bshen@pku.edu.cn)

Evidence of Type-II Band Alignment in III-nitride Semiconductors: Experimental and theoretical investigation for $In_{0.17}Al_{0.83}N$/GaN heterostructures

Jiaming Wang[1], Fujun Xu[1], Xia Zhang[1], Wei An[1], Xin-Zheng Li[1,2], Jie Song[1], Weikun Ge[1,4], Guangshan Tian[1], Jing Lu[1], Xinqiang Wang[1,2], Ning Tang[1], Zhijian Yang[1], Wei Li[3], Weiying Wang[3], Peng Jin[3], Yonghai Chen[3] & Bo Shen[1,2]

[1]State Key Laboratory of Artificial Microstructure and Mesoscopic Physics, School of Physics, Peking University, Beijing 100871, China, [2]Collaboration Innovation Center of Quantum Matter, Beijing 100084, China, [3]Key Laboratory of Semiconductor Materials Science and Beijing Key Laboratory of Low-dimensional Semiconductor Materials and Devices, Institute of Semiconductors, Chinese Academy of Sciences, Beijing 100083, China, [4]Department of Physics, Tsinghua University, Beijing 100084, China.

Type-II band alignment structure is coveted in the design of photovoltaic devices and detectors, since it is beneficial for the transport of photogenerated carriers. Regrettably, for group-III-nitride wide bandgap semiconductors, all existing devices are limited to type-I heterostructures, owing to the unavailable of type-II ones. This seriously restricts the designing flexibility for optoelectronic devices and consequently the relevant performance of this material system. Here we show a brandnew type-II band alignment of the lattice-matched $In_{0.17}Al_{0.83}N$/GaN heterostructure from the perspective of both experimental observations and first-principle theoretical calculations. The band discontinuity is dominated by the conduction band offset ΔE_C, with a small contribution from the valence band offset ΔE_V which equals 0.1 eV (with E_{VBM}^{AlInN} being above E_{VBM}^{GaN}). Our work may open up new prospects to realize high-performance III-Nitrides optoelectronic devices based on type-II energy band engineering.

Band alignment at heterojunctions plays a vital role in semiconductor physics and devices, as the spatial distribution of carriers determines the physical characteristics, *e.g.* the light emission intensity and recombination lifetime. For light emitting devices, carrier confinement of both holes and electrons in the same region is beneficial[1,2]; while for photovoltaic devices and detectors, spatial separation of photogenerated carriers is favourable[3]. It is noticed that in group-III-nitride semiconductors, type-II band alignment heterostructures have never been reported thus far, implying that all the devices are designed based on type-I band structures. Taking the two well-studied systems, *i.e.* the $Al_xGa_{1-x}N$/GaN and $In_xGa_{1-x}N$/GaN heterostructures as examples, both of them have type-I band alignment and therefore their applications on photovoltaic devices are quite unfavorable. On the other hand, the $In_xAl_{1-x}N$/GaN system, which has been less studied, does have the potential to make type-II heterostructures, considering the relative band alignment of InN, AlN and GaN.

As a matter of fact, $In_xAl_{1-x}N$ has drawn much attention owing to its attractive characteristics, such as large refractive index contrast and polarization mismatch with respect to GaN. More importantly, this ternary compound can be in-plane lattice matched to GaN with In composition of 0.17–0.18[4], making it a promising candidate for high reflectivity crack-free distributed Bragg reflectors (DBRs)[5] and high electron mobility transistors[6]. Besides, it also shows great potentials in near-infrared intersubband transition devices, ultraviolet optical confinement laser diodes (LDs)[6].

In spite of its potential to be type-II heterostructure as mentioned, and the fundamental importance in optoelectronic devices, an accurate measurement on the band alignment of the $In_xAl_{1-x}N$/GaN heterostructure is, however, still lacking. As far as the standard X-ray photoelectron spectroscopy (XPS) measurements are concerned, corrections on the direct experimental results must be made, owing to the existence of large polarization effects[7,8]. Since one needs to acknowledge the uncertainty existed in such a numerical treatment of this correction, additional verifications are therefore necessary. In this work, we systematically study the band alignment of lattice-matched $In_{0.17}Al_{0.83}N$/GaN by combining XPS and delicate optical studies, *i.e.* photolumi-

Table I | Structural parameters of the samples for XPS and PL measurements

	No.	Sample structure	In composition x (%)	InAlN thickness (nm)	GaN thickness (nm)
Series I	A	$In_xAl_{1-x}N$ epilayer	17.3	1	2000
	B	$In_xAl_{1-x}N$ epilayer	17.3	20	2000
	C	GaN	/	/	2000
Series II	D	$In_xAl_{1-x}N$/GaN MQWs	17.3	1.5	4
	E	$In_xAl_{1-x}N$/GaN MQWs	17.3	2.2	4
	F	$In_xAl_{1-x}N$/GaN MQWs	17.3	3	4

nescence (PL) and time-resolved PL (TRPL). In addition, theoretical investigation on this issue is also carried out using the first-principle calculations. From the perspective of both experimental observations and theoretical results, a brandnew type-II band alignment is confirmed in this kind of heterostructure.

Two series of epitaxial samples were prepared, whose structures are summarized in Table I. Series I were studied to investigate the valence band offset (VBO) by XPS measurements, while Series II including multiple quantum wells (MQWs) with different structural parameters were used to provide evidence for type-II alignment from spatially indirect PL transition.

Figure 1 shows the schematic energy band alignment for the $In_{0.17}Al_{0.83}N$/GaN interface labeled with binding energy determined by XPS from Series I samples. The valence band offset ΔE_V can be estimated from Equation 1:

$$\Delta E_V = \Delta E_{CL} + (E_{Al2p}^{InAlN} - E_{VBM}^{InAlN}) - (E_{Ga2p}^{GaN} - E_{VBM}^{GaN}) \quad (1)$$

where $\Delta E_{CL} = (E_{Ga2p}^{GaN} - E_{Al2p}^{AlInN})$ is the binding energy difference for the measured Al 2p and Ga 2p core levels of $In_{0.17}Al_{0.83}N$/GaN heterostructure (sample A). The two terms in the form of $(E_{core\ \ level}^{Material} - E_{VBM}^{Material})$ are the separations in binding energies between the core level and valence band maximum (VBM) of $In_xAl_{1-x}N$ or GaN as bulk materials, which can be obtained from the samples of the 20-nm-thick $In_{0.17}Al_{0.83}N$ (sample B) and 2-μm-thick GaN (sample C) epilayers, respectively. The obtained XPS binding energy levels for InAlN and GaN are presented in the figure corresponding to the left and right Y axes alternately. For convenience, the values of $(E_{core\ \ level}^{Material} - E_{VBM}^{Material})$ are labeled in place. It is worth noting that the polarization-induced internal fields in the $In_{0.17}Al_{0.83}N$ layer result in the bending of the energy band. As a consequence, the apparent E_{Al2p}^{InAlN} spectrum is actually given by integrating the spectra (the dot lines) from the points of each depth along the bent core level, as schematically illustrated in the inset. That makes it deviated from the actual level at the interface. Hence careful numerical treatments[8] were performed to correct the deviation, and the corrected results are displayed as the red lines in the figure. The value of ΔE_V is then calculated to be 0.1 eV (with E_{VBM}^{AlInN} being above E_{VBM}^{GaN}). Since the energy bandgap of $In_{0.17}Al_{0.83}N$ has been measured to be 3.9 eV in our previous report[9], and the bandgap of GaN is well known to be 3.4 eV, the conduction band offset ΔE_C is estimated to be 0.6 eV, therefore suggesting a type-II band alignment for the $In_{0.17}Al_{0.83}N$/GaN heterostructure, and the large part of the band discontinuity is taken by ΔE_C.

To verify the type of the band alignment, the effect of the spatial distribution of carriers in $In_{0.17}Al_{0.83}N$/GaN MQWs structures has been investigated. As shown in the inset of Fig. 2, the schematic band diagram for type-II MQWs is depicted taking into account of the polarization field and the band offset obtained above. Electrons and holes are separately located in the GaN and InAlN layers. There are thus two electron-hole recombination channels, labeled as Channel 1 and 2, and their relative intensity depends on the width of the well and barrier. For a wide GaN well and a comparatively narrower $In_xAl_{1-x}N$ barrier, the PL recombination via Channel 1 should be the predominant process. Moreover, when the GaN width is kept constant, the emission peak via Channel 1 should exhibit energy redshift with increasing width of the $In_xAl_{1-x}N$ barrier, which is entirely different from the case in type-I MQWs; while the peak via Channel 2 remains unchanged. It is noticed that in type-I structures, such as AlGaN/GaN MQWs, the energy of the MQWs emis-

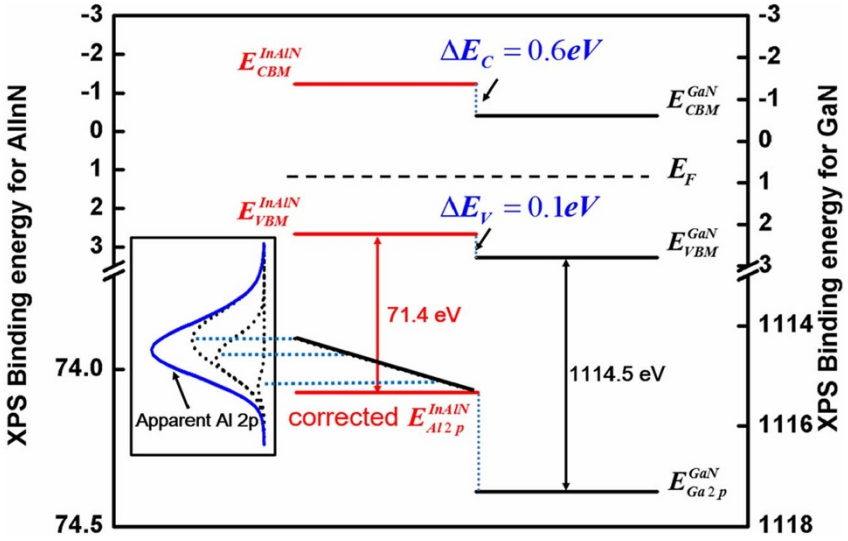

Figure 1 | Schematic energy band alignment for the $In_{0.17}Al_{0.83}N$/GaN interface. The black lines represent the measured XPS binding energy for core levels and VBM from Series I samples, while the red lines show the corrected results by numerical treatments for $In_{0.17}Al_{0.83}N$. The inset illustrates the deviation of the apparent E_{Al2p}^{InAlN} spectrum (the blue line) from the actual level (the red line labeled as corrected E_{Al2p}^{InAlN}) at the interface caused by the polarization-induced internal field in $In_{0.17}Al_{0.83}N$ layer.

sion peak is independent of the barrier width within a small variation as reported in literatures[10], due to the fact that the polarization electrical field in the wells should not be significantly affected by the barrier width.

Low-temperature (8 K) PL measurements are conducted under the same conditions for Series II samples D–F (MQWs with 4 nm-thick GaN well but various barrier widths), which are elaborately designed to enhance the recombination probability from Channel 1, as shown in Fig. 2. The dominant emission peak, whose intensity linearly increases with the excitation density (not shown here), corresponds to excitonic transition from the MQWs of samples. The full width at half maximum (FWHM) of the peaks is 30–50 meV, presenting excellent optical quality. Meanwhile, a peak with a lower emission intensity at around 3.47 eV appears, resulting from the underneath GaN template[10]. The most notable feature in the figure is the energy redshift (~0.13 eV) of the MQWs emission peaks as the barrier width increases from 1.5 to 3.0 nm, which is in line with the characteristic of the recombination via Channel 1, as discussed above. Taking the values of the polarization-induced internal fields in $In_xAl_{1-x}N$/GaN MQWs measured by Zhou *et al*[11], the variation of the energy band diagram is plotted for two different barrier widths (1.5 and 3 nm, respectively) in the inset of Fig. 2. It can be found that the effective recombination emission energy lowers down as the barrier width increases, and the estimated shift of 0.09 eV (assuming that the polarization-induced internal field in the barrier is 0.6 MV/cm[11]) is close to the measured PL redshift amount. In addition, with increasing the barrier width, the intensity of the MQWs emission peaks drastically decreases. The reason is that as the $In_{0.17}Al_{0.83}N$ barrier is thickened, the spatial separation of electron and hole wave functions becomes greater, resulting in smaller overlap that reduces the oscillator strength, and consequently the radiative recombination[12]. That is also a typical character of type-II MQWs.

We further investigate the dynamics of the radiative recombination in samples D–F by TRPL[7]. Fig. 3 shows the PL decay process for emission peaks of the three different MQWs. The measurements were carried out at 8 K to avoid non-radiative recombination which is generally frozen at that temperature, and thus to ensure that the decay curves mainly reveal the characteristics of the radiative one. Biexponential function is used to fit the normalized decay curves, and the obtained lifetime values of τ_1 and τ_2 are shown in the figure. The longer one, τ_2, which dominates the process, corresponds to the radiative recombination lifetime of the lowest excited states in the quantum wells, while the shorter τ_1 is thought to involve some energy relaxation processes for hot carriers to the first excited state. When the $In_{0.17}Al_{0.83}N$ barrier width is increased from 1.5 to 3.0 nm, there is an increase of the characteristic time τ_2 from 1.72 to 22.1 ns. This indicates a reduction of the radiative recombination probability which is reciprocal of the radiative lifetime. That again indicates the reduced overlap of electron and hole wave functions with increasing the barrier width. More importantly, it is worth noting that the value of τ_2 is much greater than the typical ones in other III-nitride quantum wells, such as in type-I $Al_xGa_{1-x}N$/GaN MQWs with an approximate well width of 4 nm, whose radiative recombination lifetimes at around 8 K are generally a few hundred picoseconds[13,14], one or two magnitudes of order less than what we obtained for the $In_{0.17}Al_{0.83}N$/GaN MQWs. The long life time strongly verifies the greater spatial separation of electrons and holes in the latter, which is consistent with the expectations for type-II MQWs.

To better understand this band alignment of the $In_{0.17}Al_{0.83}N$/GaN heterostructures, we further performed first-principle calculations using the density functional theory for this structure with a series of indium compositions[15]. The band offset is obtained by comparing the ionization potential, which is determined by the energy difference between two exact band positions, *i.e.* the VBM and the vacuum level. Taking GaN as the reference, the relative VBM position of $In_xAl_{1-x}N$ with different indium composition (x varying from 0 to 0.6) is shown in Fig. 4. Further larger compositions are out of interest in the present work. From this figure, it is clear that the VBM of the $In_xAl_{1-x}N$ alloy moves up in a monotonous yet non-linear manner with x in the indium compositions studied. There is an intersection with the GaN line at around x = 0.1, which indicates a transition from type-I band alignment for the heterostructure when x is less than 0.1 to type-II band alignment when x is greater than 0.1. For the special interested case of $In_{0.17}Al_{0.83}N$ alloy, its VBM is about 0.1 eV above the GaN one, indicating a type-II band alignment, which is consistent with the above experimental results. We also note

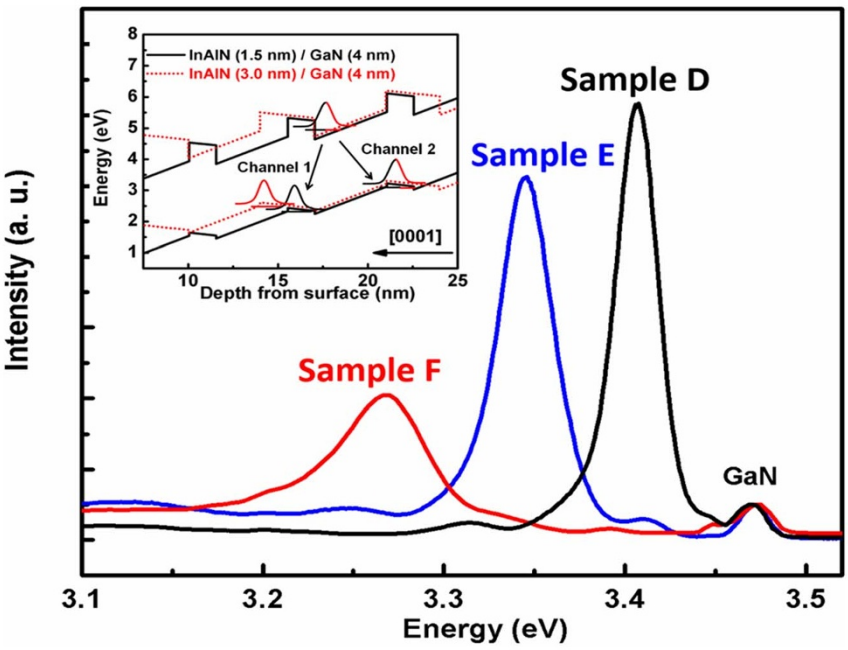

Figure 2 | Low-temperature PL spectra for samples D-E. The inset shows the schematic band diagram for type-II $In_{0.17}Al_{0.83}N$/GaN MQWs with different barrier width (black lines for 1.5 nm and red dots for 3 nm). For convenience, the quantum well labeled with electron wave function is manually aligned.

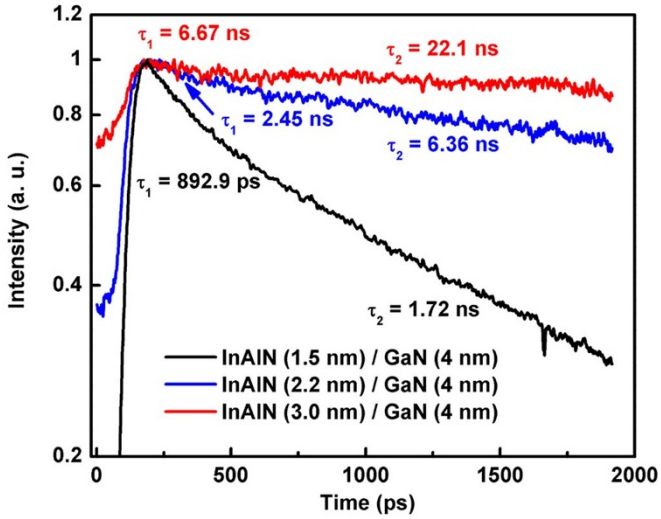

Figure 3 | PL decay process for emission peaks of the MQWs with different barrier thickness (samples D-F) at 8 K. The obtained lifetimes $\tau_1$and τ_2 are shown in place. It can be found τ_2 dominates the process.

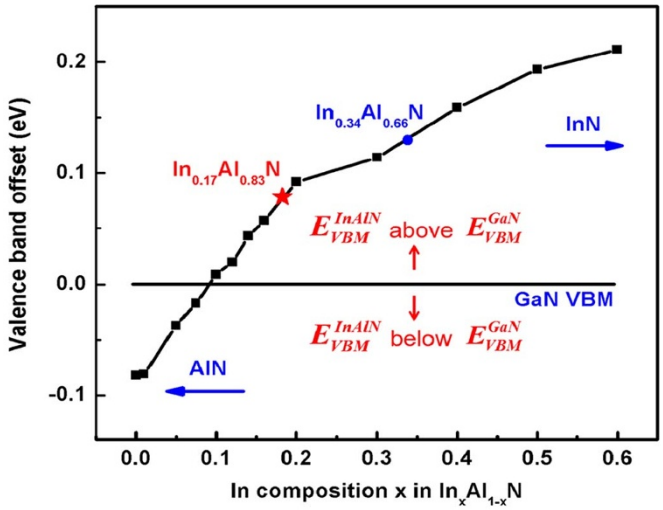

Figure 4 | The relative VBM position of $In_xAl_{1-x}N$ with different indium composition x. The VBM of GaN (the black horizontal line) is taken as the reference (0 eV). The red star shows the result of $In_{0.17}Al_{0.83}N$, while the blue dot represents the data of $In_{0.34}Al_{0.66}N$ from Ref. 17.

that an earlier theoretical calculation from Wang *et al.* for $In_{0.34}Al_{0.66}N$ presents a VBM at 0.11 eV above that of the GaN[16], which fits well to our curve in Fig. 4.

In summary, the band alignment of lattice-matched $In_{0.17}Al_{0.83}N$/GaN heterointerface has been studied by means of XPS, PL measurements and theoretical calculation. Type-II band alignment is confirmed in this kind of heterostructures. The band discontinuity is dominated by the conduction band offset ΔE_C, with a small contribution from the valence band offset ΔE_V, which equals 0.1 eV (with E_{VBM}^{AlInN} above E_{VBM}^{GaN}). We expect that this work opens up new prospects to realize high-performance III-nitride applications in optoelectronic devices, such as photodiodes, solar cells, and electron blocking layers in blue and green light-emitting diodes.

Methods

Samples Preparation. The samples studied here (listed in Table I) were $In_{0.17}Al_{0.83}N$ epilayers and 8 periods $In_{0.17}Al_{0.83}N$/GaN MQWs grown on 2-in. (0001) sapphire substrates by means of metal organic chemical vapor deposition (MOCVD), using a Thomas Swan close coupled showerhead system. After the growth of a 2-μm-thick unintentionally doped GaN template at 1040°C, the wafer was cooled down to 790°C for growing $In_{0.17}Al_{0.83}N$ epilayers and MQWs under N_2 ambient. The structural and compositional information for the samples is acquired by high resolution x-ray diffraction, as reported elsewhere[17].

X-ray Photoelectron Spectroscopy. The precise XPS measurements were performed by Imaging Photoelectron Spectrometer system (Kratos Analycital Axis Ultra), using a monochromatic Al-Kα x-ray source (1486.6 eV). The binding energy of relevant levels was obtained by adjusting the C 1s core-level peak position to 284.8 eV for each sample surface.

Optical Measurements. PL were excited by a 325 nm He-Cd laser (KIMMON IK 3301R-G), and related spectra were recorded using a monochromator/spectrograph system (Zolix Omni-λ 500). For TRPL measurements, a frequency-tripled mode-locked Ti: sapphire fs laser (COHERENT Mira HP-F Laser) with an excitation wavelength of 267 nm and a streak camera (OPTRONIS SC101) was used. The repetition rate and excitation density of the laser were 76 MHz and approximately 40 Wcm^{-2}, meanwhile the overall time resolution of the spectroscopic system is less than 16 ps. The decay curves are fitted by biexponential function

$$I(t) = A_1 \exp\left(-\frac{t}{\tau_1}\right) + A_2 \exp\left(-\frac{t}{\tau_2}\right) \quad (2)$$

where the processes corresponding to $\tau_1$and τ_2 were analyzed in this work.

First-principle Calculations. The calculations were performed using the density functional theory as implemented in CASTEP. For computational convenience, cubic zinc-blende (ZB) structures are applied instead of the wurzite (WZ) ones as the band structures at the Γ point are similar[16], that means the position of VBM and CBM are accurate in direct bandgap III-nitride semiconductors. The slab model is used[18,19], in which the supercells containing 12 atomic layers and more than 15 Å-thick vacuum are obtained by cleaving the bulk materials on the (001) surface. As the supercell shape and volume fixed, the position of internal atoms are optimized with a force tolerance 0.01 eV/Å. An energy cutoff of 350 eV and a $5 \times 5 \times 1$ k-point sampling for the Brillouin zone are used in both the geometry optimization and band structure calculations. For the $In_xAl_{1-x}N$ binary compound, the virtual crystal approximation (VCA) is used and the valence *d* electrons are suppressed in the indium pseudo-potential to guarantee a stable iteration of convergence[20]. It is worth noting that the error introduced by these approximations is investigated by comparing AlN and $In_{0.01}Al_{0.99}N$,where a 0.1 eV hopping is observed on their ionization potentials. This value of 0.1 eV is then used as a scissor operator to shift the ionization potentials calculated by VCA and this pseudo-potential in $In_xAl_{1-x}N$ for other compositions.

1. Ponce, F. A. & Bour, D. Nitride-based semiconductors for blue and green light-emitting devices. *Nature* **386**, 351–359 (1997).
2. Khan, A., Balakrishnan, K. & Katona, T. Ultraviolet light-emitting diodes based on group three nitrides. *Nat. Photonics* **2**, 77 (2008).
3. McDonald, S. A. *et al.* Solution-processed PbS quantum dot infrared photodetectors and photovoltaics. *Nat. Mater.* **4**, 138 (2005).
4. Lorenz, K. *et al.* Anomalous ion channeling in AlInN/GaN bilayers: determination of the strain state. *Phys. Rev. Lett.* **97**, 085501 (2006).
5. Carlin, J.-F. & Ilegems, M. High-quality AlInN for high index contrast Bragg mirrors lattice matched to GaN. *Appl. Phys. Lett.* **83**, 668–670 (2003).
6. Butte, R. *et al.* Current status of AlInN layers lattice-matched to GaN for photonics and electronics. *J. Phys. D: Appl. Phys.* **40**, 6328–6344 (2007).
7. Chichibu, S. F. *et al.* Origin of defect-insensitive emission probability in In-containing (Al,In,Ga)N alloy semiconductors. *Nat. Mater.* **5**, 810–816 (2006).
8. Akazawa, M. *et al.* Measurement of valence-band offsets of InAlN/GaN heterostructures grown by metal-organic vapor phase epitaxy. *J. Appl. Phys.* **109**, 013703 (2011).
9. Wang, J. M. *et al.* Indium compositional homogeneity in In0.17Al0.83N epilayers grown by metal organic chemical vapor deposition. *Appl. Phys. Express* **5**, 101002 (2012).
10. Shin, Eun-joo, Li, J., Lin, J. Y., & Jiang, H. X. Barrier-width dependence of quantum efficiencies of GaN/AlxGa1-xN multiple quantum wells. *Appl. Phys. Lett.* **77**, 1170–1172 (2000).
11. Zhou, L. *et al.* Measurement of polarization-induced electric fields in GaN/AlInN quantum wells. *Appl. Phys. Lett.* **101**, 251902 (2012).
12. Meynadier, M.-H. *et al.* Indirect-direct anticrossing in GaAs-AlAs superlattices induced by an electric field: evidence of Γ-X mixing. *Phys. Rev. Lett.* **60**, 1338–1341 (1988).
13. Lefebvre, P. *et al.* Time-resolved photoluminescence as a probe of internal electric fields in GaN-(GaAl)N quantum wells. *Phys. Rev. B* **59**, 15363 (1999).
14. Kim, H. S. *et al.* Piezoelectric effects on the optical properties of GaN/AlxGa1-xN multiple quantum wells. *Appl. Phys. Lett.* **73**, 3426–3428 (1998).
15. Segall, M. D. *et al.* First-principles simulation: ideas, illustrations and the CASTEP code. *J. Phys.: Condens. Matter* **14**, 2717 (2002).
16. Wang, F. *et al.* Effects of the wave function localization in AlInGaN quaternary alloys. *Appl. Phys. Lett.* **91**, 061125 (2007).
17. Miao, Z. L. *et al.* Strain effects on InxAl1-xN crystalline quality grown on GaN templates by metalorganic chemical vapor deposition. *J. Appl. Phys.* **107**, 043515 (2010).

18. Jiang, H. & Shen, Y. C. Ionization potentials of semiconductors from first-principles. *J. Chem. Phys.* **139**, 164114 (2013).
19. Lang, N. D. & Kohn, W. Theory of metal surfaces: work function. *Phys. Rev. B* **3**, 1215 (1971).
20. Bellaiche, L. & Vanderbilt, D. Virtual crystal approximation revisited: application to dielectric and piezoelectric properties of perovskites. *Phys. Rev. B* **61**, 7877 (2000).

Acknowledgments

This work was supported by National Basic Research Program of China (Nos. 2012CB619300, 2012CB921304 and 2013CB934600), National Natural Science Foundation of China (Grant Nos. 11174008, 61361166007 and 11275008), and the Research Fund for the Doctoral Program of Higher Education in China (Grant No. 20100001120012).

Author contributions

J.W. and F.X. designed the experiments. J.W., F.X., J.S. and Z.Y. grew the samples. J.W., X.Z. and J.S. collected data and performed related analysis. W.L., W.W., P.J. and Y.C. performed TRPL measurements. W.A. and X.Z.L. carried out the first-principle calculations. W.G., J.L., G.T., X.W., N.T. and B.S. supervised the study. J.W., F.X., X.Z.L. and W.G. wrote the manuscript. All the authors discussed the results and commented on the manuscript.

Additional information

Competing financial interests: The authors declare no competing financial interests.

How to cite this article: Wang, J. *et al.* Evidence of Type-II Band Alignment in III-nitride Semiconductors: Experimental and theoretical investigation for $In_{0.17}Al_{0.83}N$/GaN heterostructures. *Sci. Rep.* **4**, 6521; DOI:10.1038/srep06521 (2014).